Generalized Design of Position-Based Bilateral Control Parameterized by Complementary Sensitivity Function

Akihiro Suzumura, *Member, IEEE*, and Yasutaka Fujimoto, *Senior Member, IEEE*

***Abstract*—This paper proposes a generalized two-channel position-based bilateral controller architecture parameterized with a complementary sensitivity function. With this theoretical framework, we formalize a control architecture that simplifies and extends the controllers commonly employed in industrial applications. Furthermore, we propose a control architecture that divides the transfer matrices to allow multiple sensors for feedback controllers. This method allows us to use sensors such as encoders and accelerometers to enhance disturbance suppression performance while minimizing input oscillations small.**

***Index Terms*—Accelerometers, complementary-sensitivity-based parameterization, encoders, position-based bilateral control, two-channel bilateral control.**

I. Introduction

BILATERAL control shares motion information such as position, velocity, acceleration, and force measurements between master and slave devices to synchronize movement. Bilateral control will be a key technique for future human-support technologies [1]. Specifically, it can be used in medical applications such as robotic forceps to support precise surgical operations with motion information [2]. Motion-copying systems are another potential application for bilateral control systems [3]. Once motion data are recorded during a task performed with a bilateral controller, the motion can be repeated *ad nauseam* by the same controller. This technique can allow skillful human motion to be recorded and reproduced.

Researchers have taken approaches with bilateral control. Some studies deal with master/slave transmission as a two-port model [4], and another group proposed transparency and passivity-based control [5]. A study has also shown that passivity-based controllers can maintain stable operation under various conditions [6]. Parallel force/position teleoperation control has been proposed in a system composed of position and force controllers [7]. Also, several studies have implemented disturbance observer-based (DOB) control for bilateral systems [8], [9]. In these methods, the DOB achieves a robust acceleration control and a reaction force observer (RFOB) is employed for force sensing [10], [11]. By using RFOB, reaction forces can be estimated without a force sensor, and the available sensing bandwidth is wide [12].

The above-mentioned bilateral control approaches can be divided into several categories. For example, the two-channel approach shares two data channels between the master and slave sides for position and force monitoring, and the four-channel approach uses four data streams, which include position and force information, for both sides. All the applications described at the beginning of this section use four channels. This approach is popular because the four-channel approach can achieve high-performance haptic transmission and position synchronization. However, a force sensor cannot always be mounted on both master and slave devices due to cost limitations, so the realization of high-performance haptic transmission with a two-channel bilateral controller with only position signal is of considerable interest. In addition, communication channels are limited in some cases, such as when motion needs to be communicated to remote actuators. Considerable communicated data can lead to delays; therefore, communicated data should be as compressed as possible.

Data compression has been investigated using discrete cosine transform [13], and another study employed a delta-sigma modulator for haptic data quantization [14]. Other studies have tried to reduce the amount of feedback information to realize bilateral control with only two data channels. For example, a conceptual scheme for bilateral control only using position information was proposed in [15]. Several studies have focused on passivity-based controller design with time delays, such as a position–position control architecture [16], [17]. Another study proposed a control structure that depends on internal models for position-based two-channel control with time delays and external disturbances [18]. These approaches are not intended to deal with haptic transmission but instead suppress the effects of time delays, system uncertainties, and disturbances; therefore, these approaches achieve only position synchronization and transmit

Manuscript received March 29, 2017; revised July 6, 2017, October 1, 2017, and December 21, 2017; accepted February 13, 2018. Date of publication March 8, 2018; date of current version June 26, 2018. *(Corresponding author: Akihiro Suzumura.)*

A. Suzumura is with the Department of Electrical and Computer Engineering, Yokohama National University, Yokohama 240-8501, Japan (e-mail: suzumura-akihiro-gx@ynu.jp).

Y. Fujimoto is with the Department of Electrical and Computer Engineering, Yokohama National University, Yokohama 240-8501, Japan, and also with the Kanagawa Institute of Industrial Science and Technology, Kanagawa 243-0435, Japan (e-mail: fujimoto@ynu.ac.jp).

Color versions of one or more of the figures in this paper are available online at http://ieeexplore.ieee.org.

Digital Object Identifier 10.1109/TIE.2018.2811359

force data less accurately than four-channel approaches. In contrast, a two-channel approach that realizes position synchronization and force transmission with position information alone is proposed in [19] and [20]. This control system is structured such that the position information is fed back mutually between the master and slave sides. With this method, haptic transmission can be achieved while keeping the amount of communicated data small.

After we summarize the theory behind bilateral controllers in Section II, Section III rederives the two-channel bilateral control design from the theoretical architecture of a complementary-sensitivity-function-based controller (Q-based controller). Then, in Section IV, we report the performance improvements gained with multiple feedback channels that we achieved by dividing the transfer matrix. A control system that achieves both position synchronization and force transmission can be realized with the general architecture of Q-based controller design. Our controllers are derived from generalized expressions, which enables the construction of controllers with a range of plant expressions. Owing to the generality of our approach, we can clarify two specific controller structures below. One is the multiple-input multiple-output (MIMO) formulation, which is equivalent to conventional bilateral controllers [19], [20], and the other is the multiple-input single-output (MISO) formulation, which simplifies conventional controllers without deteriorating performance. The MISO formulation is only possible with the rederived Q-based approach that we presented in Section III; therefore, our rederivation meaningfully simplifies controller design. The control-system design proposed in Section III is extended by the parameterization of the complementary sensitivity function, which can be derived once we divide the transfer matrix, which enables multiple-sensor feedback. This new controller structure can be derived based on the rederived Q-based approach. Thereby, the rederivation is also meaningful for further extension of the controller design.

With our proposed control framework, it is possible to feedback not only position information but also acceleration information. For conventional four-channel architectures, a method of detecting acceleration information in addition to position information to improve the performance of the control system has been studied [21]–[23]. In this paper, we propose a control system that improves the performance of two-channel controllers with similar sensor configurations. A previous study proposed a terminal sliding-mode control and neural-network-based adaptive scheme that uses a similar feedback configuration; however, the objective of this study was not to improve haptic transmission but to manage time delays, system uncertainties, and disturbances [24]. Unlike that approach, our proposal aims at improving haptic transmission performance.

II. Bilateral Control Formalism

First, we explain the dynamics of the master/slave device to be controlled. For the devices on either master/slave side, we chose a single-axis rotary actuator for simplicity. The general scheme of a bilateral controller is shown in Fig. 1. The master

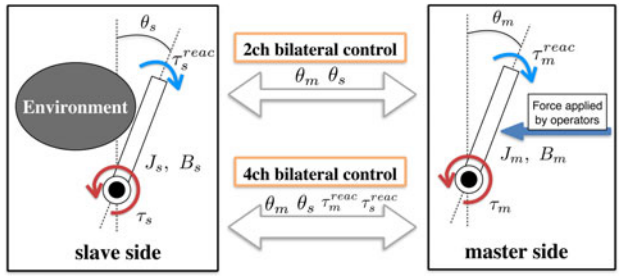

Fig. 1. Explanatory figure of bilateral control.

device is manipulated manually, and then, the slave device is synchronized with the master device by the controller, which can then interact with its environment. Then, the dynamics of the master and slave devices are described in the following equations:

$$J_m\ddot{\theta}_m + B_m\dot{\theta}_m = \tau_m - d_m \tag{1}$$

$$J_s\ddot{\theta}_s + B_s\dot{\theta}_s = \tau_s - d_s \tag{2}$$

where subscript m denotes master and s denotes slave. $J_\circ$ is the motor inertia, $B_\circ$ is the viscous friction coefficient, $\theta_\circ$ is the motor rotation angle, $\tau_\circ$ is the motor torque, and $d_\circ$ is the disturbance torque, and disturbance $d_\circ$ includes reaction force $\tau_\circ^{\mathrm{reac}}$ from environments and nonlinear friction $\tau_\circ^{\mathrm{fric}}$.

Bilateral control has two main objectives. A controller must achieve position synchronization by minimizing the difference between the master and slave positions, and must satisfy the law of action and reaction by minimizing the sum of forces applied by the master and slave devices. These control objectives can be expressed in the time domain as follows:

$$\theta_m - \theta_s = 0 \tag{3}$$

$$\left.\begin{aligned}\tau_m + \tau_s^{\mathrm{reac}} &= 0\\ \tau_s + \tau_m^{\mathrm{reac}} &= 0\end{aligned}\right\} \rightarrow \tau_m^{\mathrm{reac}} + \tau_s^{\mathrm{reac}} = 0. \tag{4}$$

A control law that realizes the above-mentioned objectives in the Laplacian domain is given by the following equations [8], [9]:

$$\tau_m = \frac{1}{2}J_{mn}\left((K_p + K_d s)\theta_e - K_f\tau_e\right) + \hat{d}_m \tag{5}$$

$$\tau_s = \frac{1}{2}J_{sn}\left(-(K_p + K_d s)\theta_e - K_f\tau_e\right) + \hat{d}_s. \tag{6}$$

In these equations, $\theta_e(s) = \theta_s(s) - \theta_m(s)$ is the position error and $\tau_e(s) = \hat{\tau}_m^{\mathrm{reac}}(s) + \hat{\tau}_s^{\mathrm{reac}}(s)$ is the force error between the master and slave sides. $\hat{\tau}_\circ^{\mathrm{reac}}$ is the reaction torque estimated by RFOB or the torque sensor, and $\hat{d}_\circ$ is the disturbance torque estimated by the DOB. In this case, as both position and force data are fed back mutually, the controllers use four channels. Note here that force data are essential for the four-channel bilateral controller. On the other hand, the two-channel bilateral control architecture we describe below requires only position data; thereby, in what follows, we will refer to the control law as a position-based bilateral controller.

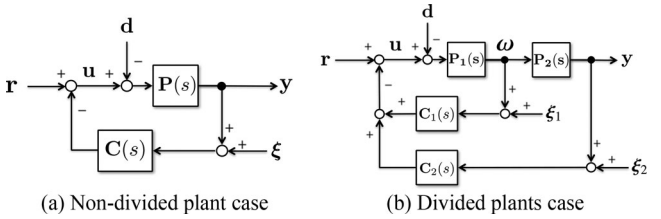

(a) Non-divided plant case (b) Divided plants case

Fig. 2. Block diagrams of control design method for a proposed bilateral control system.

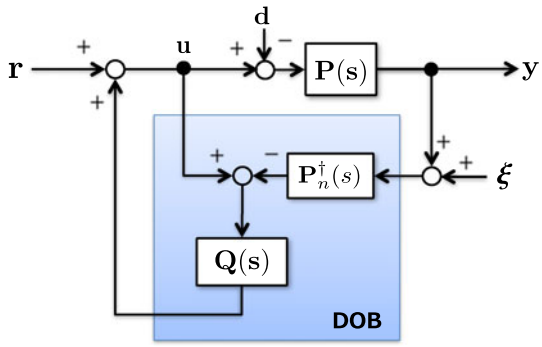

Fig. 3. DOB-type equivalent block diagram of two-DoF control.

III. Redesign of Position-Based Bilateral Controller Using Q-Based Control Framework

In this section, a general procedure for designing a position-based bilateral control system using Q-parametrization is described.

A. Q-Based Controller

First, we describe a first control architecture. For a block diagram of the control architecture, see Fig. 2(a). Then, let us take an input $\mathbf{u} \in \mathbb{R}^n$ and an output $\mathbf{y} \in \mathbb{R}^m$. The target value $\mathbf{r}$ and the observation noise $\boldsymbol{\xi}$ have the same dimensions as those of output, and the disturbance $\mathbf{d}$ has the same dimension as that of input. As a result, the controlled plant and the controller are $\mathbf{P} \in \mathbb{R}(s)^{m\times n}$ and $\mathbf{C} \in \mathbb{R}(s)^{n\times m}$. In our controller derivation, we consider only the case of n ≥ m. Controllers for the case of n < m can be derived similarly and the characteristics of the control system are nearly equal. First, we obtain the input transfer function $\mathbf{u}(s)$ of the two-DoF control system in the following equations:

$$\mathbf{u} = \boldsymbol{\Delta}^{-1}\left(\mathbf{r} + \mathbf{CPd} - \mathbf{C}\boldsymbol{\xi}\right) \tag{7}$$

$$\Delta = \mathbf{I} + \mathbf{CP}. \tag{8}$$

Then, the output transfer function $\mathbf{y}(s)$ can be derived with the following equation:

$$\mathbf{y} = \mathbf{P}\boldsymbol{\Delta}^{-1}\left(\mathbf{r} - \mathbf{d} - \mathbf{C}\boldsymbol{\xi}\right). \tag{9}$$

Subsequently, let us define $\mathbf{S}(s)$ as a transfer function matrix from $\mathbf{r}(s)$ to $\mathbf{u}(s)$ and define $\mathbf{Q}(s)$ as a transfer function matrix from $\mathbf{d}(s)$ to $\mathbf{u}(s)$ as follows:

$$\mathbf{S} \equiv \boldsymbol{\Delta}^{-1} = (\mathbf{I} + \mathbf{CP})^{-1} \tag{10}$$

$$\mathbf{Q} \equiv \boldsymbol{\Delta}^{-1}\mathbf{CP} \tag{11}$$

where $\mathbf{S}(s)$ is called the sensitivity function matrix and $\mathbf{Q}(s)$ is called the complementary sensitivity function matrix. Herein, the relationship $\mathbf{Q}(s) = \mathbf{I} - \mathbf{S}(s)$ holds. Solving the above-mentioned equations for $\mathbf{C}(s)$, a controller is obtained with the following equation:

$$\mathbf{C} = (\mathbf{I} - \mathbf{Q})^{-1}\mathbf{QP}^{\dagger}. \tag{12}$$

In (12), the operator † expresses the Moore–Penrose pseudoinverse, which is defined as follows:

$$\mathbf{P}^{\dagger} \equiv \mathbf{P}^{T}(\mathbf{PP}^{T})^{-1} \ (n \geq m). \tag{13}$$

In this way, a two-DoF controller can be parameterized based on the complementary sensitivity function matrix. In an actual controller, the nominal transfer function matrix $\mathbf{P}_n(s)$ is used.

Next, we describe characteristics of this control architecture. The internal stability of the control system against an external signal can be discussed with the matrix in the following equation:

$$\begin{bmatrix}\mathbf{u}\\ \mathbf{y}\end{bmatrix} = \begin{bmatrix}\mathbf{I}-\mathbf{Q} & \mathbf{Q} & -\mathbf{QP}_n^{\dagger}\\ \mathbf{P}_n(\mathbf{I}-\mathbf{Q}) & -\mathbf{P}_n(\mathbf{I}-\mathbf{Q}) & -\mathbf{P}_n\mathbf{QP}_n^{\dagger}\end{bmatrix}\begin{bmatrix}\mathbf{r}\\ \mathbf{d}'\\ \boldsymbol{\xi}\end{bmatrix} \tag{14}$$

where $\mathbf{d}'(s) = \mathbf{d}(s) + \left(\mathbf{P}^{\dagger}(s) - \mathbf{P}_n^{\dagger}(s)\right)\mathbf{y}(s)$ is the sum of modeling error and input side disturbance. In case of servo-control design, free parameters are chosen such that they force the tracking error to zero based on the following equation:

$$\lim_{t\to\infty}\mathbf{e} = \lim_{t\to\infty}(\mathbf{r}-\mathbf{y}) = \lim_{s\to 0} s\Big(\big(\mathbf{I}-\mathbf{P}_n(\mathbf{I}-\mathbf{Q})\big)\mathbf{r} + \mathbf{P}_n(\mathbf{I}-\mathbf{Q})\mathbf{d}' + \mathbf{P}_n\mathbf{QP}_n^{\dagger}\boldsymbol{\xi}\Big). \tag{15}$$

Finally, as shown in Fig. 3, this control system is equivalent to a DOB control architecture. From the above, the stability and servo-tracking conditions can be determined by $\mathbf{Q}(s)$ parameterization; therefore, we will refer to these controllers as "Q-based" in what follows.

B. Design of a Q-Based Bilateral Controller Based on MIMO-Systems Formulation

1) Controller Configuration: Parameter selection based on the MIMO system formulation is described. The master/slave system naturally has two inputs and two outputs. Then, we can rearrange the dynamics as in the following equation:

$$\begin{bmatrix}\theta_m\\ \theta_s\end{bmatrix} = \begin{bmatrix}\frac{1}{J_m s^2 + B_m s} & 0\\ 0 & \frac{1}{J_s s^2 + B_s s}\end{bmatrix}\left(\begin{bmatrix}\tau_m'\\ \tau_s'\end{bmatrix} - \begin{bmatrix}\tau_m^{\mathrm{reac}}\\ \tau_s^{\mathrm{reac}}\end{bmatrix}\right). \tag{16}$$

The actual input is $\tau_{\circ}(s) = \tau_{\circ}'(s) + \tau_{\circ}^{ff}(s)$, and $\tau_{\circ}^{ff}$ is a feed-forward term for canceling nonlinear disturbances such as $\tau_{\circ}^{\mathrm{fric}}$, except for $\tau_{\circ}^{\mathrm{reac}}$. Let us assume that nonlinear disturbances are canceled by $\tau_{\circ}^{ff}$. Some cancellation error is unavoidable; however, it can be suppressed by the feedback controller, as we will

discuss below. From (16), the identities can be obtained by the following equations:

$$\mathbf{y} = \begin{bmatrix} y_1 & y_2 \end{bmatrix}^T = \begin{bmatrix} \theta_m & \theta_s \end{bmatrix}^T \tag{17}$$

$$\mathbf{u} = \begin{bmatrix} u_1 & u_2 \end{bmatrix}^T = \begin{bmatrix} \tau'_m & \tau'_s \end{bmatrix}^T \tag{18}$$

$$\mathbf{d} = \begin{bmatrix} d_1 & d_2 \end{bmatrix}^T = \begin{bmatrix} \tau_m^{\text{reac}} & \tau_s^{\text{reac}} \end{bmatrix}^T \tag{19}$$

$$\xi = \begin{bmatrix} \xi_1 & \xi_2 \end{bmatrix}^T \tag{20}$$

$$\mathbf{P} = \begin{bmatrix} P_1 & 0 \\ 0 & P_2 \end{bmatrix} = \begin{bmatrix} \frac{1}{J_m s^2 + B_m s} & 0 \\ 0 & \frac{1}{J_s s^2 + B_s s} \end{bmatrix}. \tag{21}$$

Then, $\mathbf{Q}(s)$ is defined as $\mathbf{Q}(s) \equiv \begin{bmatrix} Q_{11}(s) & Q_{12}(s) \\ Q_{21}(s) & Q_{22}(s) \end{bmatrix}$. The control objectives are position synchronization and satisfying the law of action/reaction between the master and slave devices. In this controller architecture, both control objectives are indirectly realized based on the design choices of free parameters $\mathbf{Q}(s)$. This implies that we do not treat the controller design problem as a servo-tracking control problem in MIMO configuration. Thereby, we can neglect a target term $\mathbf{r}(s)$. In this case, each element of the resulting feedback controller $\mathbf{C}(s) = \begin{bmatrix} C_{11}(s) & C_{12}(s) \\ C_{21}(s) & C_{22}(s) \end{bmatrix}$ can be obtained in the following equations:

$$C_{11} = \frac{1}{P_{1n}} \frac{(1 - Q_{22})Q_{11} + Q_{12}Q_{21}}{(1 - Q_{11})(1 - Q_{22}) - Q_{12}Q_{21}} \tag{22}$$

$$C_{12} = \frac{1}{P_{2n}} \frac{Q_{12}}{(1 - Q_{11})(1 - Q_{22}) - Q_{12}Q_{21}} \tag{23}$$

$$C_{21} = \frac{1}{P_{1n}} \frac{Q_{21}}{(1 - Q_{11})(1 - Q_{22}) - Q_{12}Q_{21}} \tag{24}$$

$$C_{22} = \frac{1}{P_{2n}} \frac{(1 - Q_{11})Q_{22} + Q_{12}Q_{21}}{(1 - Q_{11})(1 - Q_{22}) - Q_{12}Q_{21}}. \tag{25}$$

2) Condition Derivation: To realize position synchronization between the master and the slave, the condition $\theta_e = \theta_m - \theta_s = 0$ needs to be satisfied. Thereby, we consider the following limit as follows:

$$\lim_{t\to\infty}(y_1 - y_2) = \lim_{s\to 0} s\,(y_1 - y_2) = \lim_{s\to 0} s\mathbf{I}_p\mathbf{y} \tag{26}$$

where $\mathbf{I}_p = \begin{bmatrix} 1 & -1 \end{bmatrix}$. The output transfer characteristics of a closed system can be obtained from (14). Then, the following relation holds:

$$\mathbf{I}_p\mathbf{y} = -\mathbf{I}_p\Big(\mathbf{P}_n(\mathbf{I} - \mathbf{Q})\mathbf{d}' + \mathbf{P}_n\mathbf{Q}\mathbf{P}_n^{\dagger}\boldsymbol{\xi}\Big). \tag{27}$$

In (27), the first term on the right-hand side is related to the position synchronization. To synchronize the device's position, the free parameter $\mathbf{Q}(s)$ should be set to suppress the effects of disturbances.

Next, we describe how our design architecture satisfies the law of action/reaction between the master and slave sides indirectly with free parameters design. To satisfy the law of action/reaction, the master or slave side needs to generate forces that correspond to the force applied to the slave or master side, that is, the conditions $\tau_{e1} = \tau'_m + \tau_s^{\text{reac}} = 0$ and $\tau_{e2} = \tau'_s + \tau_m^{\text{reac}} = 0$ need to be satisfied. Therefore, we consider the following limit as follows:

$$\lim_{t\to\infty}\begin{bmatrix} u_1 + d_2 \\ u_2 + d_1 \end{bmatrix} = \lim_{s\to 0} s\begin{bmatrix} u_1 + d_2 \\ u_2 + d_1 \end{bmatrix} = \lim_{s\to 0} s\left(\mathbf{u} + \bar{\mathbf{I}}\mathbf{d}\right) \tag{28}$$

where $\bar{\mathbf{I}}$ is an antidiagonal unit matrix $\bar{\mathbf{I}} = \begin{bmatrix} 0 & 1 \\ 1 & 0 \end{bmatrix}$. The input transfer characteristics of a closed system can be obtained from (14). Then, $\mathbf{u}(s) + \bar{\mathbf{I}}\mathbf{d}(s)$ can be rearranged as in the following equation:

$$\mathbf{u} + \bar{\mathbf{I}}\mathbf{d} = \begin{bmatrix} \bar{\mathbf{I}} + \mathbf{Q} & -\mathbf{Q}\mathbf{P}_n^{\dagger} \end{bmatrix}\begin{bmatrix} \mathbf{d} \\ \boldsymbol{\xi} \end{bmatrix} + \mathbf{Q}\left(\mathbf{P}^{\dagger} - \mathbf{P}_n^{\dagger}\right)\mathbf{y}. \tag{29}$$

In (29), the first term on the right-hand side is related to the law of action/reaction realization. To satisfy this law, the free parameter $\mathbf{Q}(s)$ should be set to suppress the effects of disturbances. Also, as the second term of the equation expresses the difference between a real plant and a nominal plant, performance will deteriorate with large modeling errors. However, this error is suppressed in our design by multiplying the term by $\mathbf{Q}(s)$. In ideal situations, the law of action/reaction can be satisfied without force-data feedback. However, nonlinear effects such as friction, gravity, centrifugal force, and Coriolis force need to be compensated for separately in a feedforward manner. In this case, the compensation error from the nonlinear elements also affects the system through the term $\mathbf{Q}(s)$. Note that DOB/RFOB-based control architectures commonly require the identification of nonlinear elements and plant model parameters for both DOB and RFOB. With these architectures, parameters of them must be preidentified. Then, the effects of nonlinear elements are subtracted online from the disturbance estimated by DOB for RFOB, and plant model parameters are used for both DOB and RFOB. As a result, the compensation error affects performance in the same fashion as it does in our proposed approach. Finally, (27) and (29) can be summarized under the condition that $\mathbf{P}(s) = \mathbf{P}_n(s)$, with the following equation:

$$\begin{bmatrix} y_1 - y_2 \\ u_1 + d_2 \\ u_2 + d_1 \end{bmatrix} = \begin{bmatrix} -P_1(1 - Q_{11}) - P_2Q_{21} & P_1Q_{12} + P_2(1 - Q_{22}) \\ Q_{11} & 1 + Q_{12} \\ 1 + Q_{21} & Q_{22} \end{bmatrix}$$
$$\begin{bmatrix} -Q_{11} + \frac{P_2}{P_1}Q_{21} & -\frac{P_1}{P_2}Q_{12} + Q_{22} \\ -\frac{Q_{11}}{P_1} & -\frac{Q_{12}}{P_2} \\ -\frac{Q_{21}}{P_1} & -\frac{Q_{22}}{P_2} \end{bmatrix}\begin{bmatrix} d_1 \\ d_2 \\ \xi_1 \\ \xi_2 \end{bmatrix}. \tag{30}$$

3) Free Parameter Design: Next, we introduce our proposed parameter-selection criteria. By introducing $Q_{12}(s) = -Q'_{12}(s)$ and $Q_{21}(s) = -Q'_{21}(s)$, the resulting controller architecture described in (22)–(25) corresponds with the controller architecture obtained in [19]. Thereby, the conventional controller design is a special case of our controller design method. Our parameter choice criteria are described by the

following equations:

$$Q_{11} = Q_{22} = 0 \tag{31}$$

$$Q_{12} = -Q'_{12} = -\frac{a_1 s + a_0}{s^3 + a_2 s^2 + a_1 s + a_0} \tag{32}$$

$$Q_{21} = -Q'_{21} = -\frac{b_1 s + b_0}{s^3 + b_2 s^2 + b_1 s + b_0} \tag{33}$$

where $Q_{12}(s)$ and $Q_{21}(s)$ are chosen as third-order low-pass Butterworth filters with cutoff frequencies ω_{c12} and ω_{c21}. Relative order of the filter is chosen to satisfy the internal stability of closed-loop transfer function matrices in (14), and to satisfy that all outputs of (30) converge to zero for a certain class of disturbances. Note that any types of low-pass filters are available for $Q_{12}(s)$ and $Q_{21}(s)$ if the above conditions are satisfied. The objective of this paper is not to indicate the filter design but the effectiveness of our proposed framework; therefore, the commonly used Butterworth filters are employed for the fundamental verifications. These criteria present the challenge of a tradeoff between disturbance suppression and noise suppression, which can also be found in the conventional DOB-based approach. This effect can be seen in (27) and (29). The higher the cutoff frequency value of $Q_{12}(s)$ and $Q_{21}(s)$ is set, the lower are the position and force errors between the master and slave sides. However, higher values of the cutoff frequencies of $Q_{12}(s)$ and $Q_{21}(s)$ invite more noise in the output observations. Moreover, the modeling error that tends to be biased in a high-frequency region affects the performance with higher values of the cutoff frequencies. This means that there is a tradeoff relationship between suppressing disturbances and suppressing modeling error effects. This is another limitation of this framework; however, the effect is not so problematic compared with noise effects. Thereby, the problem is not explicitly considered for the design in this paper, that is, the cutoff frequency is determined as high as possible until the noise effect becomes problematic.

C. Controller Design Based on MISO System Formulation

1) Controller Configuration: Next, let us consider position synchronization achieved indirectly through free-parameter design choices. Herein, the output of the control system is selected as $\theta_m(s) - \theta_s(s)$ to achieve position synchronization. Then, the transfer function matrix from input to output is expressed as follows:

$$y = \theta_m - \theta_s = \begin{bmatrix} \frac{1}{J_m s^2 + B_m s} & -\frac{1}{J_s s^2 + B_s s} \end{bmatrix} (\mathbf{u} - \mathbf{d}). \tag{34}$$

From (34), we can obtain the following equation:

$$\mathbf{P} = \begin{bmatrix} P_1 & -P_2 \end{bmatrix} = \begin{bmatrix} \frac{1}{J_m s^2 + B_m s} & -\frac{1}{J_s s^2 + B_s s} \end{bmatrix}. \tag{35}$$

In this case, observation noise can be expressed as $\xi(s) = \xi_1(s) - \xi_2(s)$, where $\xi_1(s)$ and $\xi_2(s)$ are the noises defined in (20). Then, let us define $\mathbf{Q}(s)$ as we did above. As described above, the system to be controlled is MISO. To achieve position synchronization between the master and the slave, the target value $r(s)$ of the control system is always set to zero. In this case, each element of the resulting feedback controller $\mathbf{C}(s) = [C_1(s)\ C_2(s)]^T$ can be obtained with the following equations:

$$C_1 = -\frac{P_1\Big(Q_{11}(Q_{22}-1) - Q_{12}Q_{21}\Big) + P_2 Q_{12}}{\left({P_1}^2 + {P_2}^2\right)\Big((1-Q_{11})(1-Q_{22}) - Q_{12}Q_{21}\Big)} \tag{36}$$

$$C_2 = \frac{P_2\Big(Q_{22}(Q_{11}-1) - Q_{12}Q_{21}\Big) + P_1 Q_{21}}{\left({P_1}^2 + {P_2}^2\right)\Big((1-Q_{11})(1-Q_{22}) - Q_{12}Q_{21}\Big)}. \tag{37}$$

Note here that the MISO configuration involves fewer controllers than the MIMO configuration.

2) Condition Derivation: Unlike the MIMO case, position synchronization between the master and the slave in the MISO case can be realized by considering a servo-tracking problem. Then, the equation for position synchronization can be derived from the servo condition (15). The equation for satisfying the law of action/reaction is simply given by (29). Finally, (15) and (29) can be summarized by using the definitions (34) and (35) under the condition that $\mathbf{P}(s) = \mathbf{P}_n(s)$ and $r(s) = 0$, as shown in the following equation:

$$\begin{bmatrix} y_1 - y_2 \\ u_1 + d_2 \\ u_2 + d_1 \end{bmatrix} = \begin{bmatrix} -P_1(1-Q_{11}) - P_2 Q_{21} & P_1 Q_{12} + P_2(1-Q_{22}) \\ Q_{11} & 1 + Q_{12} \\ 1 + Q_{21} & Q_{22} \end{bmatrix} \begin{bmatrix} -\frac{P_1(P_1 Q_{11} - P_2 Q_{21}) - P_2(P_1 Q_{12} - P_2 Q_{22})}{{P_2}^2 + {P_1}^2} \\ -\frac{P_1 Q_{11} - P_2 Q_{12}}{{P_2}^2 + {P_1}^2} \\ -\frac{P_1 Q_{21} - P_2 Q_{22}}{{P_2}^2 + {P_1}^2} \end{bmatrix} \begin{bmatrix} d_1 \\ d_2 \\ \xi_1 - \xi_2 \end{bmatrix}. \tag{38}$$

Compared with (30), the transfer functions against observation noise $\xi_1(s)$ and $\xi_2(s)$ are different.

3) Free Parameter Design: Next, we introduce a parameter selection criterion. Parameters can be selected in the same fashion as they were for the MIMO configuration. In this case, all outputs of (38) converge to zero for a certain class of disturbances. Interestingly, the controllers in (36) and (37) can be simplified under the condition that $Q_{11}(s) = Q_{22}(s) = 0$, $Q(s) = Q'_{12}(s) = Q'_{21}(s)$, and $P(s) = P_1(s) = P_2(s)$, as in the following equation:

$$C_{1,2} = \pm\frac{Q}{2P(1-Q)} \tag{39}$$

where one controller is to be implemented. This is a special case of the controllers in (36) and (37). Though their range of applications is limited, these controllers are significantly simplified without deterioration of the control performance. Note that this performance-preserving simplification is possible only with the MISO configuration, which appears with the introduction of a position-based bilateral controller design using the Q-based control framework, ensuring the novelty of our proposed controller framework.

IV. Performance Improvement With Multiple-Information Feedback From Dividing the Transfer Function Matrix

In this section, we introduce a novel expression for the complementary sensitivity function that we derive by dividing the transfer function matrix. This proposal builds on the single-input and multiple-output configuration (SIMO) proposed in [26]. This transfer function matrix division enables us to use two feedback signals for position-based bilateral control. For example, combining position and acceleration signals is useful in improving performance at disturbance estimation. The position and acceleration-integrated disturbance observer controller utilizes combined signals to widen the bandwidth of disturbance estimation and suppression [21]. This approach is especially useful when a resolution-limited encoder is used for position detection, and allows a high-frequency-band accelerometer to be used. Although this is a useful method to improve the performance of DOB control, it can only be utilized with four-channel systems. On the other hand, our proposed method generates a controller architecture that utilizes acceleration information alone for two-channel bilateral control. Our method can minimize the effects of observation noise and enhance the controllers disturbance-suppression performance. The details of our design procedures are presented next.

A. Q-Based Controller With Divided Plants

First, we derive a controller by dividing the transfer function matrix. For the block diagram, refer Fig. 2(b). Then, we consider the input $\mathbf{u} \in \mathbb{R}^n$, the output $\mathbf{y} \in \mathbb{R}^m$, and the intermediate variable newly obtained by dividing the transfer function $\boldsymbol{\omega} \in \mathbb{R}^m$. The target value is $\mathbf{r} \in \mathbb{R}^m$, the observation noise accompanying the observation of the intermediate variable is $\boldsymbol{\xi}_1 \in \mathbb{R}^m$, the noise induced from observing the output is $\boldsymbol{\xi}_2 \in \mathbb{R}^o$, and the disturbance is $\mathbf{d} \in \mathbb{R}^n$. Then, the controlled object and the controller are $\mathbf{P}_1 \in \mathbb{R}(s)^{n\times m}$, $\mathbf{P}_2 \in \mathbb{R}(s)^{o\times n}$, $\mathbf{C}_1 \in \mathbb{R}(s)^{m\times n}$, and $\mathbf{C}_2 \in \mathbb{R}(s)^{m\times o}$. Here, the input of the closed system against an external signal is obtained with the following equations:

$$\begin{aligned}\mathbf{u} = \ & \boldsymbol{\Delta}_{\text{ex}}^{-1}\big(\mathbf{r} - (\mathbf{C}_1\mathbf{P}_1 + \mathbf{C}_2\mathbf{P}_2\mathbf{P}_1)\mathbf{d} \\ & - \mathbf{C}_1\boldsymbol{\xi}_1 - \mathbf{C}_2\boldsymbol{\xi}_2\big) \qquad (40)\end{aligned}$$

$$\boldsymbol{\Delta}_{\text{ex}} = \mathbf{I} + \mathbf{C}_1\mathbf{P}_1 + \mathbf{C}_2\mathbf{P}_2\mathbf{P}_1. \qquad (41)$$

Then, the output of the closed system against an external signal is calculated with the following equation:

$$\mathbf{y} = \mathbf{P}_2\mathbf{P}_1\boldsymbol{\Delta}_{\text{ex}}^{-1}(\mathbf{r} - \mathbf{d} - \mathbf{C}_1\boldsymbol{\xi}_1 - \mathbf{C}_2\boldsymbol{\xi}_2). \qquad (42)$$

With regard to the sensitivity transfer function matrix, as there are two transfer function matrices of plants to be controlled, the two complementary sensitivity functions $\mathbf{S}_1, \mathbf{Q}_1 \in \mathbb{R}(s)^{m\times m}$ and $\mathbf{S}_2, \mathbf{Q}_2 \in \mathbb{R}(s)^{m\times m}$ can be defined. Subsequently, we choose $\mathbf{S}_1(s)$ as the transfer function matrix from $\mathbf{r}(s)$ to $\mathbf{u}(s)$ and $\mathbf{Q}_1(s)$ as the transfer function matrix from $\mathbf{d}(s)$ to $\mathbf{u}(s)$ as follows:

$$\mathbf{S}_1 \equiv \boldsymbol{\Delta}_{\text{ex}}^{-1} = (\mathbf{I} + \mathbf{C}_1\mathbf{P}_1 + \mathbf{C}_2\mathbf{P}_2\mathbf{P}_1)^{-1} \qquad (43)$$

$$\mathbf{Q}_1 \equiv \boldsymbol{\Delta}_{\text{ex}}^{-1}(\mathbf{C}_1\mathbf{P}_1 + \mathbf{C}_2\mathbf{P}_2\mathbf{P}_1) \qquad (44)$$

where the relation $\mathbf{S}_1(s) = \mathbf{I} - \mathbf{Q}_1(s)$ holds. Then, we divide (44) as follows:

$$\mathbf{Q}_1 - \mathbf{Q}_2 \equiv \boldsymbol{\Delta}_{\text{ex}}^{-1}\mathbf{C}_1\mathbf{P}_1 \qquad (45)$$

$$\mathbf{Q}_2 \equiv \boldsymbol{\Delta}_{\text{ex}}^{-1}\mathbf{C}_2\mathbf{P}_2\mathbf{P}_1. \qquad (46)$$

This definition follows the related study on SIMO systems [26]. Later, we will verify that the controller derived from the above-mentioned definition possesses the desired characteristics. Solving (45) and (46) for $\mathbf{C}_1(s)$ and $\mathbf{C}_2(s)$ leads to the controllers in the following equations:

$$\mathbf{C}_1 = (\mathbf{I} - \mathbf{Q}_1)^{-1}(\mathbf{Q}_1 - \mathbf{Q}_2)\mathbf{P}_1^{\dagger} \qquad (47)$$

$$\mathbf{C}_2 = (\mathbf{I} - \mathbf{Q}_1)^{-1}\mathbf{Q}_2\mathbf{P}_1^{\dagger}\mathbf{P}_2^{\dagger}. \qquad (48)$$

As above, the controllers can be parameterized with multiple complementary sensitivity functions. In an actual controller, the nominal transfer function matrices $\mathbf{P}_{1n}(s)$ and $\mathbf{P}_{2n}(s)$ are used.

Next, we explain the closed-loop characteristics of the obtained controllers. The internal stability matrix of the control system against an external signal is shown in the following equation:

$$\begin{bmatrix}\mathbf{u}\\ \boldsymbol{\omega}\\ \mathbf{y}\end{bmatrix} = \begin{bmatrix}\mathbf{I}-\mathbf{Q}_1 & \mathbf{Q}_1\\ \mathbf{P}_{1n}(\mathbf{I}-\mathbf{Q}_1) & -\mathbf{P}_{1n}^{\dagger}(\mathbf{I}-\mathbf{Q}_1)\\ \mathbf{P}_{2n}\mathbf{P}_{1n}(\mathbf{I}-\mathbf{Q}_1) & -\mathbf{P}_{2n}\mathbf{P}_{1n}(\mathbf{I}-\mathbf{Q}_1)\end{bmatrix}$$

$$\begin{bmatrix}-(\mathbf{Q}_1-\mathbf{Q}_2)\mathbf{P}_{1n}^{\dagger} & -\mathbf{Q}_2\mathbf{P}_{1n}^{\dagger}\mathbf{P}_{2n}^{\dagger}\\ -\mathbf{P}_{1n}(\mathbf{Q}_1-\mathbf{Q}_2)\mathbf{P}_{1n}^{\dagger} & -\mathbf{P}_{1n}\mathbf{Q}_2\mathbf{P}_{1n}\dagger\mathbf{P}_{2n}\dagger\\ -\mathbf{P}_{2n}\mathbf{P}_{1n}(\mathbf{Q}_1-\mathbf{Q}_2)\mathbf{P}_{1n}^{\dagger} & -\mathbf{P}_{2n}\mathbf{P}_{1n}\mathbf{Q}_2\mathbf{P}_{1n}^{\dagger}\mathbf{P}_{2n}^{\dagger}\end{bmatrix}\begin{bmatrix}\mathbf{r}\\ \mathbf{d}'\\ \boldsymbol{\xi}_1'\\ \boldsymbol{\xi}_2\end{bmatrix} \qquad (49)$$

where $\mathbf{d}'(s) = \mathbf{d}(s) + (\mathbf{P}_1^{\dagger}(s)\mathbf{P}_2^{\dagger}(s) - \mathbf{P}_{1n}^{\dagger}(s)\mathbf{P}_{2n}^{\dagger}(s))\mathbf{y}(s)$ is the sum of modeling error and input side disturbance, and $\boldsymbol{\xi}_1'(s) = \boldsymbol{\xi}_1(s) + (\mathbf{P}_2^{\dagger}(s) - \mathbf{P}_{2n}^{\dagger}(s))\mathbf{y}(s)$ is a term for modeling error and observation noise for the intermediate variable. Compared with the internal stability matrix of the control system in Section III, this matrix is complicated due to the introduction of an additional feedback loop. To stabilize the closed-loop system, the free parameters $\mathbf{Q}_1(s)$ and $\mathbf{Q}_2(s)$ must be chosen properly. In addition, in order to realize the servo control, free parameters should be determined with reference to the following equation:

$$\begin{aligned}\lim_{t\to\infty}\mathbf{e} = \ & \lim_{t\to\infty}(\mathbf{r}-\mathbf{y}) = \lim_{s\to 0} s\Big(\big(\mathbf{I}-\mathbf{P}_n(\mathbf{I}-\mathbf{Q})\big)\mathbf{r}\\ & + \mathbf{P}_{2n}\mathbf{P}_{1n}(\mathbf{I}-\mathbf{Q}_1)\mathbf{d}' + \mathbf{P}_{2n}\mathbf{P}_{1n}(\mathbf{Q}_1-\mathbf{Q}_2)\mathbf{P}_{1n}^{\dagger}\boldsymbol{\xi}_1'\\ & + \mathbf{P}_{2n}\mathbf{P}_{1n}\mathbf{Q}_2\mathbf{P}_{1n}^{\dagger}\mathbf{P}_{2n}^{\dagger}\boldsymbol{\xi}_2\Big). \qquad (50)\end{aligned}$$

From (49) and (50), we confirm that the relations in (45) and (46) for the complementary sensitivity function are realized as defined in our controller derivation. Moreover, the effect of external signals on the system is determined by $\mathbf{I} - \mathbf{Q}_1(s)$ for $\mathbf{d}'(s)$, $\mathbf{Q}_1(s) - \mathbf{Q}_2(s)$ for $\boldsymbol{\xi}_1'$, and $\mathbf{Q}_2(s)$ for $\boldsymbol{\xi}_2$. In other words, our divided-plant controller can increase the degrees of freedom available for the control system and allow feedback from multiple sensors, thereby adding freedom in design choices for suppressing the influences of external signals acting on the

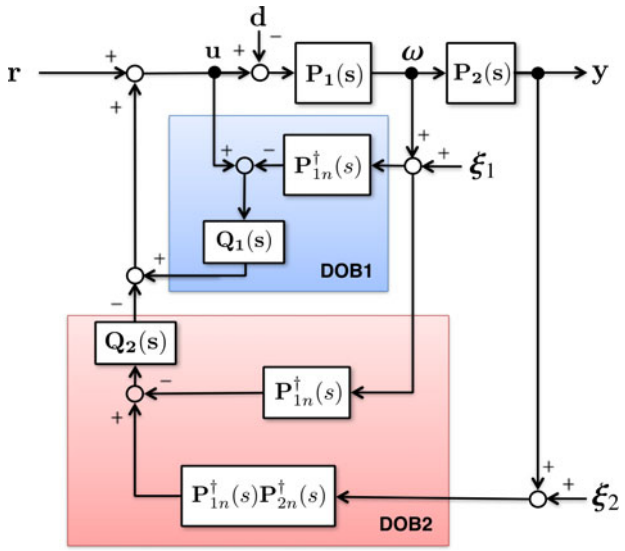

Fig. 4. Equivalent block diagram of controllers based on division of transfer function matrix.

system. Finally, as shown in Fig. 4, the controllers obtained from the divided plants have a structure with multiple equivalent DOBs. An inner DOB removes input-side disturbances and an outer DOB removes the influence of observation noise.

B. Controller Design of a Q-Based Bilateral Controller Based on MIMO Systems Formulation

1) Controller Configuration: Next, we describe parameter selection based on MIMO formulation. The output of the system and the intermediate variable $\mathbf{y}(\mathbf{s})$ and $\boldsymbol{\omega}(s)$ can be selected as in the following equations:

$$\mathbf{y} = \begin{bmatrix} y_1 \\ y_2 \end{bmatrix} = \begin{bmatrix} \theta_m \\ \theta_s \end{bmatrix} = \frac{1}{s^2}\boldsymbol{\omega} \tag{51}$$

$$\boldsymbol{\omega} = \begin{bmatrix} \omega_1 \\ \omega_2 \end{bmatrix} = \begin{bmatrix} \ddot{\theta}_m \\ \ddot{\theta}_s \end{bmatrix} = \begin{bmatrix} \frac{s}{J_m s + B_m} & 0 \\ 0 & \frac{s}{J_s s + B_s} \end{bmatrix} (\mathbf{u} - \mathbf{d}). \tag{52}$$

In this case, observation noise can be expressed as follows:

$$\boldsymbol{\xi}_1 = [\xi_1^1 \ \xi_2^1]^T \tag{53}$$

$$\boldsymbol{\xi}_2 = [\xi_1^2 \ \xi_2^2]^T. \tag{54}$$

From (51) and (52), we can derive the following equations:

$$\mathbf{P}_1 = \begin{bmatrix} P_1^1 & 0 \\ 0 & P_2^1 \end{bmatrix} = \begin{bmatrix} \frac{s}{J_m s + B_m} & 0 \\ 0 & \frac{s}{J_s s + B_s} \end{bmatrix} \tag{55}$$

$$P_2 = \frac{1}{s^2}. \tag{56}$$

Then, let us define $\mathbf{Q}_1(s) \equiv \begin{bmatrix} Q_{11}^1(s) & Q_{12}^1(s) \\ Q_{21}^1(s) & Q_{22}^1(s) \end{bmatrix}$ and $\mathbf{Q}_2(s) \equiv \begin{bmatrix} Q_{11}^2(s) & Q_{12}^2(s) \\ Q_{21}^2(s) & Q_{22}^2(s) \end{bmatrix}$. In the same fashion as with the nondivided plant case, a target term $\mathbf{r}(s)$ is neglected. In this case, eight controllers $\mathbf{C}_1 \in \mathbb{R}(s)^{2\times 2}$ and $\mathbf{C}_2 \in \mathbb{R}(s)^{2\times 2}$ must be realized. We omit the detailed expression due to space limitations.

2) Condition Derivation: Position synchronization between the master and the slave can be considered with (26). The output transfer characteristics of the closed-loop system can be obtained from (49). Therefore, the following relation holds:

$$\mathbf{I}_p\mathbf{y} = -\mathbf{I}_p\Big(\mathbf{P}_{2n}\mathbf{P}_{1n}(\mathbf{I}-\mathbf{Q}_1)\mathbf{d}' + \mathbf{P}_{2n}\mathbf{P}_{1n}(\mathbf{Q}_1-\mathbf{Q}_2)\mathbf{P}_{1n}^{\dagger}\boldsymbol{\xi}_1' + \mathbf{P}_{2n}\mathbf{P}_{1n}\mathbf{Q}_2\mathbf{P}_{1n}^{\dagger}\mathbf{P}_{2n}^{\dagger}\boldsymbol{\xi}_2\Big). \tag{57}$$

With the above-mentioned transfer function, the observation noise added to the control system $\boldsymbol{\xi}_1$ is the acceleration sensor noise on the master/slave side and $\boldsymbol{\xi}_2$ is the master/slave side encoder noise. Since the encoder introduces errors due to angle-detection quantization, quantization noise becomes a problem. In the case where the resolution is low, the noise is particularly problematic in the high-frequency range. On the other hand, the acceleration sensor introduces noise in the low-frequency to high-frequency range. Herein, errors in low-frequency measurements, such as offset errors due to deviation in calibration from temperature variations, are likely to be problematic. To achieve position synchronization, the free parameter $\mathbf{Q}_1(s)$ should be set to suppress disturbances. In addition, $\mathbf{Q}_2(s)$ can be determined to minimize the effects of observation noise.

Next, the law of action/reaction between the master and slave sides can be considered with (28). The input transfer characteristic of the closed-loop system can be obtained from (49). Then, $\mathbf{u} + \bar{\mathbf{I}}\mathbf{d}$ can be rearranged as follows:

$$\mathbf{u} + \bar{\mathbf{I}}\mathbf{d} = \begin{bmatrix} \bar{\mathbf{I}} + \mathbf{Q}_1 & -(\mathbf{Q}_1 - \mathbf{Q}_2)\mathbf{P}_{1n}^{\dagger} & -\mathbf{Q}_2\mathbf{P}_{1n}^{\dagger}\mathbf{P}_{2n}^{\dagger} \end{bmatrix} \begin{bmatrix} \mathbf{d} \\ \boldsymbol{\xi}_1' \\ \boldsymbol{\xi}_2 \end{bmatrix} + \mathbf{Q}_1(\mathbf{P}_1^{\dagger}\mathbf{P}_2^{\dagger} - \mathbf{P}_{1n}^{\dagger}\mathbf{P}_{2n}^{\dagger})\mathbf{y}. \tag{58}$$

To satisfy the law of action/reaction, the free parameter $\mathbf{Q}_1(s)$ should be determined to suppress the effects of disturbances. As in the case of two-DoF control, the second term of the equation is a modeling error that can be suppressed with $\mathbf{Q}_1(s)$. Under ideal circumstances, the law of action/reaction can be realized without feeding force information back. In both the position synchronization and the law of action/reaction cases, the effect of disturbance $\mathbf{d}'(s)$ is determined by $\mathbf{Q}_1(s)$. On the other hand, the effect of noise $\boldsymbol{\xi}_1(s)$ (accelerometer noise) is determined by $\mathbf{Q}_1(s) - \mathbf{Q}_2(s)$ and that of $\boldsymbol{\xi}_2(s)$ (encoder quantization noise) is determined by $\mathbf{Q}_2(s)$. Owing to these relations, we can utilize information from two sensors for control stabilization. Therefore, a better choice is to design parameters $\mathbf{Q}_1(s) - \mathbf{Q}_2(s)$ as a bandpass filter and $\mathbf{Q}_2(s)$ as a low-pass filter. The condition (57) and (58) can be summarized as a matrix in the same fashion as they were for the nondivided plants case under the condition that $\mathbf{P}_1(s) = \mathbf{P}_{1n}(s)$ and $\mathbf{P}_2(s) = \mathbf{P}_{2n}(s)$; however, the explicit expression is omitted due to space limitations.

3) Free Parameter Design: Next, a parameter selection criterion is introduced. Herein, let us define $Q_{12}^i(s) = -Q_{12}^{i\prime}(s)$ and $Q_{21}^i(s) = -Q_{21}^{i\prime}(s)$, where, $i = 1, 2$. Then, the parameter

choices are given by the following equations:

$$Q_{11}^i = Q_{22}^i = 0 \tag{59}$$

$$Q_{12}^i = -Q_{12}^{i\prime} = -\frac{a_{1i}s + a_{0i}}{s^3 + a_{2i}s^2 + a_{1i}s + a_{0i}} \tag{60}$$

$$Q_{21}^i = -Q_{21}^{i\prime} = -\frac{b_{1i}s + b_{0i}}{s^3 + b_{2i}s^2 + b_{1i}s + b_{0i}} \tag{61}$$

where $Q_{12}^i(s)$ and $Q_{21}^i(s)$ are chosen as third order low-pass Butterworth filters with cutoff frequencies ω_{c12}^i and ω_{c21}^i. Relative order of the filter is chosen to satisfy the internal stability and disturbance suppression condition based on (49), (57), and (58) same as nondivided plant case. Then, if the gains are determined as $\omega_{c\circ}^2 < \omega_{c\circ}^1$, the encoder noise affects the system through its low-pass filter characteristic, and the accelerometer noise affects the system through its bandpass filter characteristic.

C. Controller Design of Q-Based Bilateral Controller Based on MISO System Formulation

1) Controller Configuration: In this section, we describe parameter selection for the MISO system formulation. The output of the system and the intermediate variable, $y(s) = \theta_m(s) - \theta_s(s)$ and $\omega(s) = \ddot{\theta}_m(s) - \ddot{\theta}_s(s)$, can be selected with the following equations:

$$y = \frac{1}{s^2}\omega \tag{62}$$

$$\omega = \begin{bmatrix} \frac{s}{J_m s + B_m} & -\frac{s}{J_s s + B_s} \end{bmatrix}(\mathbf{u} - \mathbf{d}). \tag{63}$$

From the above-mentioned equations, we can derive the following equations:

$$\mathbf{P}_1 = \begin{bmatrix} P_1^1 & -P_2^1 \end{bmatrix} = \begin{bmatrix} \frac{s}{J_m s + B_m} & -\frac{s}{J_s s + B_s} \end{bmatrix} \tag{64}$$

$$P_2 = \frac{1}{s^2}. \tag{65}$$

In this case, observation noise can be expressed as $\xi_1(s) = \xi_1^1(s) - \xi_2^1(s)$ and $\xi_2(s) = \xi_1^2(s) - \xi_2^2(s)$ where $\xi_1^1(s)$, $\xi_2^1(s)$, $\xi_1^2(s)$, and $\xi_2^2(s)$ are the noises defined in (53) and (54). Then, let us define $\mathbf{Q}_1(s)$ and $\mathbf{Q}_2(s)$ as we did for the MIMO configuration. As in the case of the nondivided plant case, a target term $r(s)$ is set to zero. In this case, four controllers $\mathbf{C}_1 \in \mathbb{R}(s)^{1\times 2}$ and $\mathbf{C}_2 \in \mathbb{R}(s)^{1\times 2}$ are required. The details are omitted due to space limitations.

2) Condition Derivation: In the MISO case, position synchronization between the master and the slave can be realized by considering the servo condition (50) as introduced in the plant nondivided case. Then, the equation for satisfying the law of action/reaction is simply given by (58). The explicit expression in a matrix form is omitted due to space limitations same as the MIMO case.

3) Free Parameter Design: Next, we introduce parameter selection criteria. Parameters can be selected as they were for the MIMO system configuration. In this case, all outputs of (50) and (58) converge to zero for a certain class of disturbances. As in the nondivided plant case, controllers $\mathbf{C}_1(s) = [C_{11}(s)\ C_{12}(s)]^T$ and $\mathbf{C}_2(s) = [C_{21}(s)\ C_{22}(s)]^T$ can be simplified under the condition that $Q_{11}^1(s) = Q_{22}^1(s) = Q_{11}^2(s) = Q_{22}^2(s) = 0$, $Q_1(s) = Q_{12}^{1\prime}(s) = Q_{21}^{1\prime}(s)$, and $P_1(s) = P_1^1(s) = P_2^1(s)$, as the following equation:

$$C_{11,12} = \pm\frac{Q_1 - Q_2}{2P_1(1 - Q_1)}, C_{21,22} = \pm\frac{Q_2}{2P_1P_2(1 - Q_1)}. \tag{66}$$

In (66), two controllers are required. This is a special case of bilateral controller simplification, which preserves control performance, but it is possible only with the MISO system configuration.

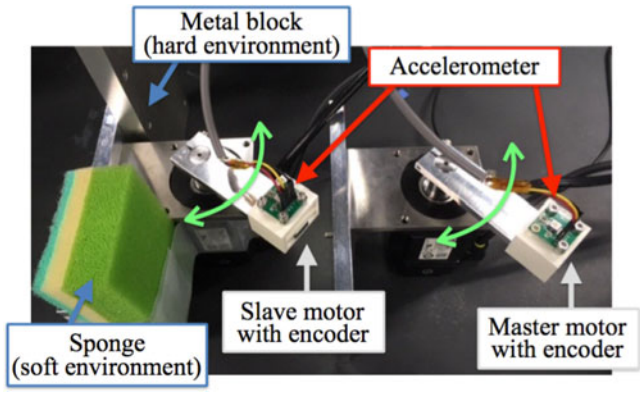

Fig. 5. Experimental setup.

V. Experiments

In this section, we present experimental results that verify the effectiveness of our proposed methods. The controlled actuator used in the experiments is shown in Fig. 5. An SGMJV-02ADA21 (Yaskawa Elec.) AC motor with encoder resolution $q_r = 2\pi/2^{20}$ rad and an SGDV-2R1F01A (Yaskawa Elec.) servo amplifier were used as actuators. In addition, an ADXL203 (Analogue Devices) was used as the acceleration sensor. The main controller was implemented on an Intel Core i7 3.7 GHz processor running on a Ubuntu Linux rt-preempt real-time kernel. The sampling time Δt for the controllers was 200 μs. Herein, for the controller design, nominal parameters of the plant were assumed, such that $J_{mn} = J_{sn} = 5.10 \times 10^{-5}$ kg·m^2 and $B_{mn} = B_{sn} = 1.77 \times 10^{-4}$ N·ms/rad. The nominal parameters were chosen through a least-square fit with experimental data. The data include velocity, acceleration, which are obtained by numerical differentiation of measured position, and torque under the condition that an M-series torque command is given. In our experiments, a soft/hard environment was used to confirm the effectiveness of our proposed methods in different contexts. An A5052 aluminum block was used for the hard environment, and a sponge was used for the soft environment.

We used two cases for our experiments. Case 1 compared conventional four-channel bilateral control (method 1) and two-channel Q-based bilateral control (method 2: MISO formulation, method 3: MIMO formulation). Case 2 compared two-channel Q-based bilateral controllers with nondivided plant (method 4: MISO formulation, method 5: MIMO formulation) and divided plants (method 6: MISO formulation, method 7: MIMO formulation) in an encoder-resolution-limited situation. Test case 1

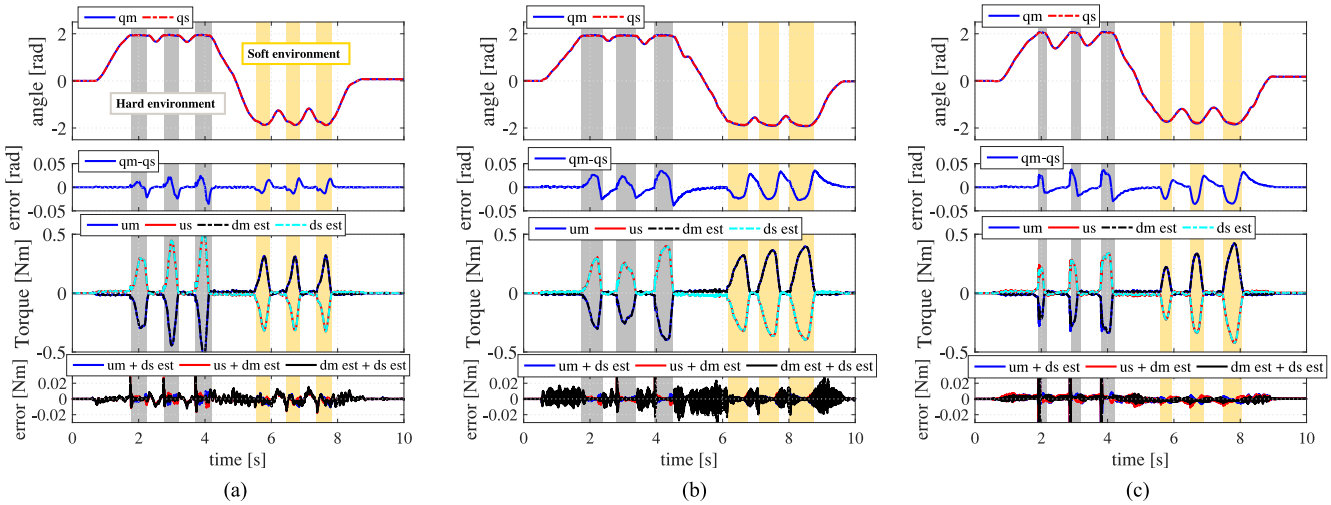

Fig. 6. Experimental results for comparing the DOB-based four-channel bilateral control [see (a)] with the proposed two-channel position-based bilateral control[see (b) and (c)]. (a) 4ch bilateral controller (method 1). (b) 2ch MISO bilateral controller (method 2). (c) 2ch MIMO bilateral controller (method 3).

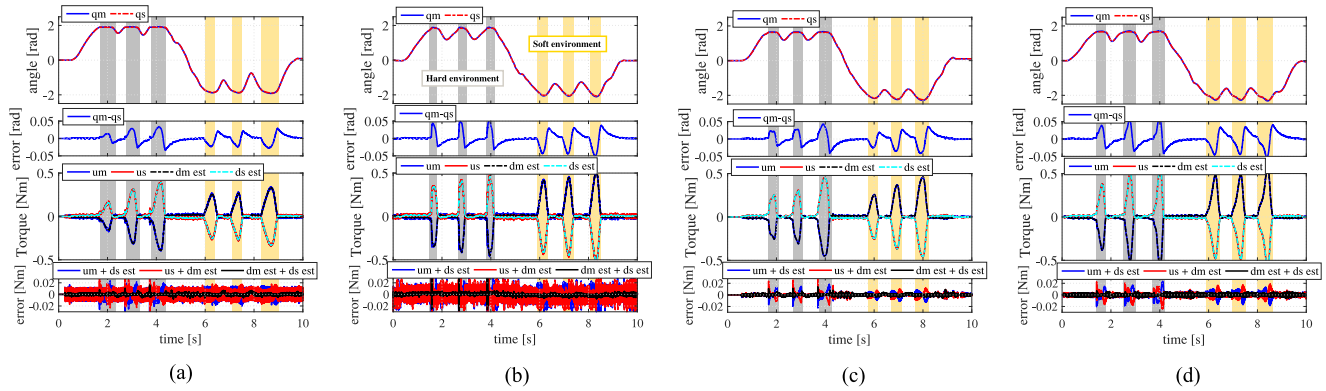

Fig. 7. Experimental results for comparing nondivided plant cases [see (a) and (b)]with divided plants cases[see (c) and (d)]. (a) 2ch MISO bilateral controller with non-divided plant (method 4). (b) 2ch MIMO bilateral controller with non-divided plant (method 5). (c) 2ch MISO bilateral controller with divided plant (method 6). (d) 2ch MIMO bilateral controller with divided plant (method 7).

indicates the effectiveness of our proposed position-based bilateral controller as compared with a conventional four-channel bilateral controller. For the four-channel bilateral controller shown in (5) and (6), $K_p = 7000$, $K_d = 300$, $K_f = 5000$, and the DOB/RFOB cutoff frequencies $\omega_{\mathrm{DOB}} = \omega_{\mathrm{RFOB}} = 700$ rad/s were used. For the proposed bilateral controller, the cutoff frequency $\omega_c = \omega_{c12} = \omega_{c21} = 700$ rad/s was used. In this test, the cutoff frequency of the proposed bilateral controller was set to be the same as the DOB cutoff frequency of the four-channel bilateral controller. Test case 2 indicates the effectiveness of our proposed position-based bilateral controller with divided plants. Herein, resolution of the encoder is intentionally lowered to 12 000 ppr to simulate the resolution-limited case. For a bilateral controller with nondivided plants, the cutoff frequency $\omega_c = 700$ rad/s was used. Then, for bilateral controller with divided plant, cutoff frequencies $\omega_{c1} = \omega^1_{c12} = \omega^1_{c21} = 700$ rad/s and $\omega_{c2} = \omega^2_{c12} = \omega^2_{c12} = 300$ rad/s were used. In this situation, the relation $\omega_c = \omega_{c1}$ holds; therefore, disturbance–suppression performance is expected to be the same. However, the effect of quantization noise from encoders can be reduced by lowering the value of ω_{c2}. For test case 2, the RFOB cutoff frequency $\omega_{\mathrm{RFOB}} = 300$ rad/s was used to ensure a fair comparison. The results of cases 1 and 2 are shown in Figs. 6 and 7(a)–(c). The top plots show position responses, the second plots show position errors, the third plots show force responses, and the bottom plots show force errors. Here, $q_\circ$ denotes position, $u_\circ$ denotes input, and $d_\circ$ denotes the reaction force of the master and slave sides. Our experimental results are evaluated quantitatively with root mean square (RMS) and maximum errors in Tables I and II.

Fig. 6(a)–(c) indicates that both the conventional and proposed controllers achieve position/force regulation. Moreover, Tables I and II show that the force errors of our proposed controller are almost equal to or smaller than the conventional method. We emphasize that the force-regulation performance of the proposed method is superior to that achieved with four-channel bilateral control, even without direct force feedback.

TABLE I
RMS ERROR OF EACH RESULT

Method	θ_e $= \theta_m - \theta_s$ [$\times 10^{-2}$ rad]	τ_{e1} $= \tau'_m + \hat{\tau}_s^{\mathrm{reac}}$ [$\times 10^{-3}$ N·m]	τ_{e2} $= \tau'_s + \hat{\tau}_m^{\mathrm{reac}}$ [$\times 10^{-3}$ N·m]	τ_e $= \hat{\tau}_m^{\mathrm{reac}} + \hat{\tau}_s^{\mathrm{reac}}$ [$\times 10^{-3}$ N·m]
1	0.5718	2.955	3.061	3.309
2	1.250	2.750	2.454	4.328
3	1.083	4.940	3.937	2.517
4	1.039	4.584	4.624	1.367
5	1.442	8.890	8.141	2.080
6	1.091	2.434	2.473	1.102
7	1.398	3.280	3.400	1.180

TABLE II
MAXIMUM ERROR OF EACH RESULT

Method	θ_e $= \theta_m - \theta_s$ [$\times 10^{-2}$ rad]	τ_{e1} $= \tau'_m + \hat{\tau}_s^{\mathrm{reac}}$ [$\times 10^{-3}$ N·m]	τ_{e2} $= \tau'_s + \hat{\tau}_m^{\mathrm{reac}}$ [$\times 10^{-3}$ N·m]	τ_e $= \hat{\tau}_m^{\mathrm{reac}} + \hat{\tau}_s^{\mathrm{reac}}$ [$\times 10^{-3}$ N·m]
1	24.22	24.15	42.21	39.30
2	35.23	14.44	41.33	42.81
3	37.31	74.72	70.16	42.77
4	34.03	28.75	50.54	16.26
5	54.98	83.18	11.87	36.04
6	42.94	18.31	32.26	13.91
7	65.97	23.55	22.49	7.390

This finding confirms the effectiveness of our proposed method for bilateral control. However, Tables I and II also indicate that position errors of the proposed method are relatively larger compared with those of conventional methods. This is assumed to be due to the structure of the equivalent DOB modules. The conventional method uses first-order DOB modules, whereas our proposed method uses equivalent third-order DOB modules. This problem can be solved by considering minimal realization of the proposed controller, i.e., same implementation as DOB manner [10]; however, it is not discussed further in this paper. Moreover, the proposed method uses only one parameter ω_{c1}, whereas the conventional method uses five parameters K_p, K_d, K_f, ω_{DOB}, and ω_{RFOB}. Therefore, the comparison is fair in the view of the degrees of freedom afforded by the controller architectures.

Fig. 7(a)–(d) indicates that both nondivided and divided plant achieve position and force regulation. Herein, the control inputs of the nondivided plant (a) and (b) are problematic due to quantization error from the simulated low-resolution encoders. As a result, the force error oscillates quite a bit compared with the high-resolution case of Fig. 6(a)–(c). In contrast, the results of the divided plant in (c) and (d) are similar to Fig. 6(a)–(c). This can be confirmed quantitatively in Tables I and II. The position error is almost identical in both cases and force errors are reduced due to small oscillations in the input. This means that our proposed method utilizes additional accelerometers to reduce input oscillations while maintaining disturbance–suppression performance. This effect can be easily achieved within the framework of our proposed method; therefore, our proposed bilateral controller that relies on divided plants meaningfully streamlines design and implementation.

VI. CONCLUSION

This paper proposed two position-based bilateral controller frameworks parameterized by complementary sensitivity functions. First, we accomplished a generalized redesign of a position-based bilateral controller framework based on complementary sensitivity function parameterization, and then extended the controller realization by dividing the transfer function matrices. Owing to our proposed method, simplified controllers could be derived without deteriorating control performance. Then, the extended proposed method allowed us to utilize multiple sensors systematically. Experimental results validated the effectiveness of our proposed methods. As a result, we confirmed that our first simplified controller without force information realized similar performance compared with a conventional four-channel bilateral controller. Moreover, the second extended framework we proposed achieved low input oscillations with low-resolution encoders as compared with our merely simplified controller.

REFERENCES

[1] K. Ohnishi, S. Katsura, and T. Shimono, "Motion control for real-world haptics," *IEEE Ind. Electron. Mag.*, vol. 4, no. 2, pp. 16–19, Jun. 2010.
[2] S. Katsura, W. Iida, and K. Ohnishi, "Medical mechatronics – An application to haptic forceps," *Annu. Rev. Control*, vol. 29, pp. 237–245, Nov. 2005.
[3] S. Katsura, W. Yamanouchi, and Y. Yokokura, "Real-world Haptics: Reproduction of human motion," *IEEE Ind. Electron. Mag.*, vol. 6, no. 1, pp. 25–31, Mar. 2012.
[4] B. Hannaford, "A design framework for teleoperators with kinesthetic feedback," *IEEE Trans. Robot. Autom.*, vol. 5, no. 4, pp. 426–434, Aug. 1989.
[5] D. A. Lawrence, "Stability and transparency in bilateral teleoperation," *IEEE Trans. Robot. Autom.*, vol. 9, no. 5, pp. 624–637, Oct. 1993. doi: 10.1109/70.258054.
[6] B. Hannaford and Jee-Hwan Ryu, "Time-domain passivity control of haptic interfaces," *IEEE Trans. Robot. Autom.*, vol. 18, no. 1, pp. 1–10, Feb. 2002.
[7] K. Hashtrudi-Zaad and S. E. Salcudean, "Bilateral parallel force/position teleoperation control," *J. Field Robot.*, vol. 19, no. 4, pp. 155–167, Jan. 2002.
[8] S. Katsura and K. Ohnishi, "A realization of haptic training system by multilateral control," *IEEE Trans. Ind. Electron.*, vol. 53, no. 6, pp. 1935–1942, Dec. 2006.
[9] T. Shimono, S. Katsura, and K. Ohnishi, "Abstraction and reproduction of force sensation from real environment by bilateral control," *IEEE Trans. Ind. Electron.*, vol. 54, no. 2, pp. 907–918, Apr. 2007.
[10] K. Ohnishi, M.Shibata, and T.Murakami, "Motion control for advanced mechatronics," *IEEE/ASME Trans. Mechatronics*, vol. 1, no. 1, pp. 56–67, Mar. 1996.
[11] T. Murakami, F. Yu, and K. Ohnishi, "Torque sensorless control in multidegree-of-freedom manipulator," *IEEE Trans. Ind. Electron.*, vol. 40, no. 2, pp. 259–265, Apr. 1993.
[12] S. Katsura, Y. Matsumoto, and K. Ohnishi, "Modeling of force sensing and validation of disturbance observer for force control," *IEEE Trans. Ind. Electron.*, vol. 54, no. 1, pp. 530–538, Feb. 2007.
[13] E. A. Baran, A. Kuzu, S. Bogosyan, M. Gokasan, and A. Sabanovic, "Comparative analysis of a selected DCT-based compression scheme for haptic data transmission," *IEEE Trans. Ind. Informat.*, vol. 12, no. 3, pp. 1146–1155, Jun. 2016.
[14] M. Takeya, Y. Kawamura and S. Katsura, "Data reduction design based on delta-sigma modulator in quantized scaling-bilateral control for realizing of haptic broadcasting," *IEEE Trans. Ind. Electron.*, vol. 63, no. 3, pp. 1962–1971, Mar. 2016.

[15] R. Machuca, C. I. Aldana, C. Lopez-Franco and E. Nuno, "Control of bilateral teleoperators using only position measurements," in *Proc. IEEE 13th Int. Conf. Netw., Sens., Control*, Apr. 2016, pp. 1–5.
[16] J. Artigas, J.-H. Ryu, and C. Preusche, "Time domain passivity control for position-position teleoperation architectures," *Presence, Teleoper. Virtual Environ.*, vol. 19, no. 5, Oct. 2010, Art. no. 482497.
[17] M. Franken, S. Misra, and S. Stramigioli, "Stability of position-based bilateral telemanipulation systems by damping injection," in *Proc. IEEE Int. Conf. Robot. Autom.*, May 2012, pp. 4300–4306.
[18] A. Denasi, D. KostiÄ, and H. Nijmeijer, "Time delay compensation in bilateral teleoperations using IMPACT," *IEEE Trans. Control Syst. Technol.*, vol. 21, no. 3, pp. 704–715, May 2013.
[19] M. Tajiri and Y. Fujimoto, "Design of bilateral control based on complementary sensitivity function using velocity information," in *Proc. 41st Annu. Conf. IEEE Ind. Electron. Soc.*, Nov. 2015, pp. 4412–4417.
[20] M. Tajiri, P. López, and Y. Fujimoto, "Design of two-channel bilateral control systems by a transfer-function-based approach," in *IEEE Trans. Ind. Electron.*, vol. 65, no. 7, pp. 5655–5664, Jul. 2018.
[21] S. Katsura, K. Irie and K. Ohishi, "Wideband force control by position-acceleration integrated disturbance observer," *IEEE Trans. Ind. Electron.*, vol. 55, no. 4, pp. 1699–1706, Apr. 2008.
[22] C. Mitsantisuk, K. Ohishi, and S. Katsura, "Estimation of action/reaction forces for the bilateral control using Kalman filter," *IEEE Trans. Ind. Electron.*, vol. 59, no. 11, pp. 4383–4393, Nov. 2012.
[23] R. Antonello, K. Ito, and R. Oboe, "Acceleration measurement drift rejection in motion control systems by augmented-state kinematic Kalman filter," *IEEE Trans. Ind. Electron.*, vol. 63, no. 3, pp. 1953–1961, Mar. 2016.
[24] Y. Yang, C. Hua and X. Guan, "Finite time control design for bilateral teleoperation system with position synchronization error constrained," *IEEE Trans. Cybern.*, vol. 46, no. 3, pp. 609–619, Mar. 2016.
[25] T. Tsuji, K. Natori, and K. Ohnishi, "A controller design method of bilateral control system," *Eur. Power Electron. Drives*, vol. 16, no. 2, pp. 22–28, May 2006.
[26] A. Suzumura, Y. Fujimoto, T. Murakami, and R. Oboe, "A general framework for designing SISO-based motion controller with multiple sensor feedback," *IEEE Trans. Ind. Electron.*, vol. 63, no. 12, pp. 7607–7620, Dec. 2016.

Akihiro Suzumura (S'15–M'17) received the B.E., M.E., and Ph.D. degrees in electrical and computer engineering from Yokohama National University, Yokohama, Japan, in 2011, 2013, and 2017, respectively.

His research interests include robotics and mechatronics, especially on motion planning and control of compliant behavior for autonomous robots.

Yasutaka Fujimoto (S'93–M'98–SM'12) received the B.E., M.E., and Ph.D. degrees in electrical and computer engineering from Yokohama National University, Yokohama, Japan, in 1993, 1995, and 1998, respectively.

In 1998, he joined Keio University, Yokohama, Japan. Since 1999, he has been with the Faculty of Engineering, Yokohama National University, where he is currently a Professor. His research interests include actuators, robotics, manufacturing automation, and motion control.

Dr. Fujimoto is an Associate Editor for the IEEE TRANSACTIONS ON INDUSTRIAL ELECTRONICS and *IEEJ Journal of Industry Applications*. He has been a Chair for the IEEE IES Technical Committee on Sensors and Actuators in 2012–2013, 2016–2017 and an AdCom Member for the IEEE IES in 2012–2013, 2016–2018. He has served as a Program Cochair for the IEEE AMC2014, AMC2018, IEEJ SAMCON2015, and a General Cochair for the IEEJ SAMCON2016, SAMCON2017, and IEEE ICM2019. He was the recipient of the IEEE ECCE2016 Best Paper Award in 2016.